Molecular Therapy
Methods & Clinical Development
Original Article

# Engineering chimeric PCSK9 for a vaccine against atherosclerosis

Špela Malenšek,[1,2] Duško Lainšček,[1,5] Hana Esih,[1,2] Sara Orehek,[1,2] Tina Fink,[1] Anja Golob Urbanc,[1] Aleš Blinc,[3,4] and Roman Jerala[1,5]

[1]Department of Synthetic Biology and Immunology, National Institute of Chemistry, 1000 Ljubljana, Slovenia; [2]Interdisciplinary Doctoral Study of Biomedicine, Medical Faculty, University of Ljubljana, 1000 Ljubljana, Slovenia; [3]Department of Vascular Diseases, University Medical Center Ljubljana, 1000 Ljubljana, Slovenia; [4]Faculty of Medicine, Department of Internal Medicine, University of Ljubljana, 1000 Ljubljana, Slovenia; [5]Centre for Technologies of Gene and Cell Therapy, National Institute of Chemistry, 1000 Ljubljana, Slovenia

**Cardiovascular diseases, especially atherosclerosis, are the main cause of death in the whole world. The risk can be reduced by lowering the serum low-density lipoprotein cholesterol by targeting proprotein convertase 9 (PCSK9) through genome editing or neutralization by monoclonal antibodies. Vaccination against PCSK9 represents an alternative with potentially long-lasting efficacy, but must overcome the challenge of immunogenicity against the endogenous protein, which can also elicit lower antibody response due to B cell tolerance. In contrast to the previously reported weakly immunogenic PCSK9 peptides, we have developed a designed chimeric PCSK9 that maintains the surface epitopes and elicits a B cell immune response with PCSK9-specific antibodies, comparable to human-based vaccines, but eliminates the natural protein T cell epitopes and impairs self-antigen-mediated T cell cytotoxicity upon vaccination. We demonstrated that vaccination with chimera-based vaccines generates humoral immunity with a decreased T cell reactivity. In an atherosclerosis mouse model, the effect persisted over 20 weeks, as evidenced by a reduction in the circulating PCSK9 and cholesterol and a lower atherosclerotic disease burden in the aorta. This demonstrates a therapeutic improvement in atherosclerosis in an animal model and the proof-of-concept for the rational design of vaccines against endogenous proteins.**

## INTRODUCTION

Atherosclerosis is a slowly progressive inflammatory cardiovascular disease, characterized by the accumulation of lipid plaques in the lining of the arterial walls.[1] The gradual narrowing of the arteries by the lipid-rich deposits progresses over the lifetime of affected individuals and can suddenly lead to complete arterial obstruction upon in the event of rupture and subsequent arterial thrombosis. Long-term exposure to high serum cholesterol (hypercholesterolemia) is a major cause of atherosclerotic disease and associated morbidity worldwide.[2,3] Low-density lipoprotein cholesterol (LDL-C) in particular plays a key role in promoting vascular inflammation and the formation of macrophage-derived foam cells.[4]

In addition to the widely used lipid-lowering statins, the HMG-CoA reductase inhibitors,[5] which reduce the LDL-C biosynthesis, some of the advanced strategies for treating atherosclerosis involve inhibition of PCSK9, proprotein convertase subtilisin/kexin type 9, which plays a key role in LDL-C uptake.[3,6] By binding to the LDL-receptor (LDLR) and initiating its degradation via the lysosomal recycling pathway, PCSK9 increases LDL-C levels in the blood.[7] Since it acts as a negative regulator of LDLR, it represents a natural target for the treatment of hypercholesterolemia. Gain-of-function mutations in PCSK9 (e.g., D374Y, leading to severe familial hypercholesterolemia[8,9]) can increase LDL-C levels above normal and cause lipid-accelerated atherosclerosis. In contrast, natural loss-of-function mutations (e.g., Q152H, which prevents the secretion of PCSK9[9,10]), reduce LDL-C levels, protect against atherosclerosis, and have no adverse effects.[11] Various strategies have been explored to neutralize PCSK9, through the use of either monoclonal antibodies (mAbs), small interfering RNA (inclisiran), or genome editing to prevent synthesis.[12–16] Several large clinical trials have shown that inhibition of PCSK9 with mAbs leads to a significant reduction in LDL-C, making patients less susceptible to further atherosclerotic development.[13] However, the high cost and other functional limitations of mAb therapy have spurred a search for alternative approaches that could overcome these limitations (including short half-life, need for frequent administration, and high cost[17]).

Vaccination,[6,18] triggering endogenous production of specific antibodies directed against PCSK9, could provide an alternative solution to overcome these limitations, particularly if a vaccine can provide long-term efficacy without the need for a frequent revaccination and likely at a fraction of the cost of mAbs. The production of antibodies against endogenous proteins is inefficient under normal conditions due to clonal deletion of self-reactive B and T cells, a natural way to prevent systemic inflammation.[17] Self-antigens must be

Received 15 January 2025; accepted 9 July 2025;
https://doi.org/10.1016/j.omtm.2025.101535.

**Correspondence:** Roman Jerala, National Institute of Chemistry, Hajdrihova 19, 1000 Ljubljana, Slovenia.
**E-mail:** roman.jerala@ki.si

presented to the immune system as a foreign-like antigen to obtain antibodies that bind to the native target in the organism.[19] Furthermore, no unwanted cytotoxic response of $CD8^+$ T lymphocytes (CTL) must be triggered, which could cause systemic inflammation and destruction of healthy cells producing the target antigen.

Nevertheless, it may be possible to break B cell tolerance without triggering T cell cytotoxicity against cells producing the self-antigen.[17] Most PCSK9 vaccine trials to date have been based on peptide vaccines, as most B cell epitopes are smaller than linear T cell epitopes.[20,21] The combination of modified PCSK9 peptides, also conjugated to carriers,[22–26] therefore only triggered a B cell (antibody-forming) response without causing T cell cytotoxicity. Peptide antigens are generally only weakly immunogenic, as they only allow linear B cell epitopes. Proteins can have both linear and discontinuous conformational epitopes, which has been shown[27] to increase both the diversity of specific antibodies produced and the high affinity for the target protein.

Here, we developed a vaccine against PCSK9 by using the rational protein design to (re)model full-length mature PCSK9. We designed chimeric PCSK9 variants, based on human (chPCSK9) and mouse PCSK9 (chmPCSK9) that aimed to elicit a B cell response with the production of PCSK9-specific antibodies without inducing the unwanted T cell cytotoxicity. *In silico* epitope mapping[28,29] was used to predict and identify the amino acid motifs within the designed vaccine antigen that can trigger the cytotoxic T cell response. This enabled us to stimulate the B cell response, while avoiding T cell cytotoxicity, which is the hallmark of a safe and efficient vaccine against self-antigens.[20,28] Vaccination of mice with a plasmid DNA (pDNA) vaccine encoding chPCSK9 constructs decreased serum PCSK9 and total serum cholesterol, increased LDLR in the liver, and showed an antiatherogenic effect on liver lipid homeostasis in experimental animals. The lack of PCSK9-specific T cell cytotoxicity in chPCSK9-vaccinated mice is reflected in the lower levels of proinflammatory cytokines secreted by splenocytes stimulated by recombinant hPCSK9 or mPCSK9. Furthermore, we show that the antibodies induced by vaccination persist over a 24-week period, resulting in attenuation of atherosclerotic plaque progression and vascular inflammation in the aortic arches of mice.

## RESULTS

### Chimeric autologous vaccine design

According to our strategy, retention of the solvent-exposed amino acid (AA) residues of the native PCSK9 fold to present conformational epitopes and "CTL de-immunization" of the engineered PCSK9 variant were the key principles for the autologous vaccine design (Figure 1A). Therefore, we designed de-immunized chimeric PCSK9 sequences for both human and mouse homologs. First, we chose a distant PCSK9 homolog that shares less than 50% of the AA residues with the native counterpart but has a conserved 3D conformation. The *Mola mola* (Ocean sunfish) homolog was identified as a suitable candidate for transplanting solvent-exposed AA residues of human or murine PCSK9. We expected the transplanted AA residues would elicit an effective B cell response: the generation of antibodies, cross-reactive with the original human/mouse PCSK9. The "human-to-*Mola mola*" and "mouse-to-*Mola mola*" chimeras therefore represented the first draft sequences.

To avoid the reactivity of CTL against PCSK9-producing cells, we introduced the second constraint for the chimera design. To eliminate epitopes of the chimeric construct that potentially cross-react with T cells, no more than 7 AA residues may be shared between the constructed chimeras and the native PCSK9. This restriction is based on the length of the major histocompatibility complex class I (MHC class I) binding peptides (8–11 amino acids), which represent very diverse fragments of endogenously synthesized proteins in the cells.[20] Although T cell receptors (TCRs) that recognize peptides from endogenous proteins such as PCSK9 are typically clonally deleted during T cell maturation, it may still be possible to induce PCSK9-specific T cell expansion by PCSK9-derived peptides that TCRs could recognize. To limit the potential T cell autoreactivity against PCSK9-producing cells, our strategy introduced mutations into the chimeras that least affected the three-dimensional (3D) conformation of the chimeric protein so that no 8-mer peptide was identical to the corresponding wt-PCSK9 peptide.

We used the "second" draft sequences as input to the online T cell epitope prediction servers: NetMHC-4.0 and NetCTL for human-based chimera and NetH2Pan for mouse-based chimera.[29–32] The final chimeric sequence of human-based chimera did not contain any strong 8-mer MHC-class-I-interacting peptides (Table 1), and the murine chimera contained three peptides (Table 2). NetCTL predicted six CTL epitopes (Table 3) for chPCSK9 potentially capable of binding at least three different human leukocyte antigens (HLA) and 10 CTL epitopes for the human homolog, but these sequences were not consistent with NetMHC predictions. Similarly, we observed a lower number of potential MHC binding epitopes for murine chimera compared to mPCSK9 (Figure S2F). To rule out autoreactivity with endogenous proteins, we also analyzed the match of short sequences to the human and mouse proteome, using BLAST analysis. We confirmed that the only similar sequences were human/murine PCSK9 and no other targets in the human/murine proteome.

The final human-based chimera sequence, chPCSK9, differed from the native hPCSK9 sequence by 27.6% (72.4% of AAs were identical and 86.7% were similar [Figure S1A]). Mouse-based chimera, chmPCSK9, differed from mPCSK9 sequence by 25.6% (74.4% of AAs were identical and 84.3% similar [Figure S1B]).

To assess the ability of the chimeras to fold to a conformation resembling native PCSK9, the structures were predicted using AlphaFold2[33] and AlphaFold3[34] (Figure S1C). The resulting average pLDDT values for mature chain conformations were 85.4 for chPCSK9 (compared to 88.83 for hCPSK9) and 85.01 for chmPCSK (compared to 86.95 for mPCSK9) (Figure S1D). This indicates a medium to high probability for the correct conformation of the 3D models for both chimeras as well as the native homologs. The models

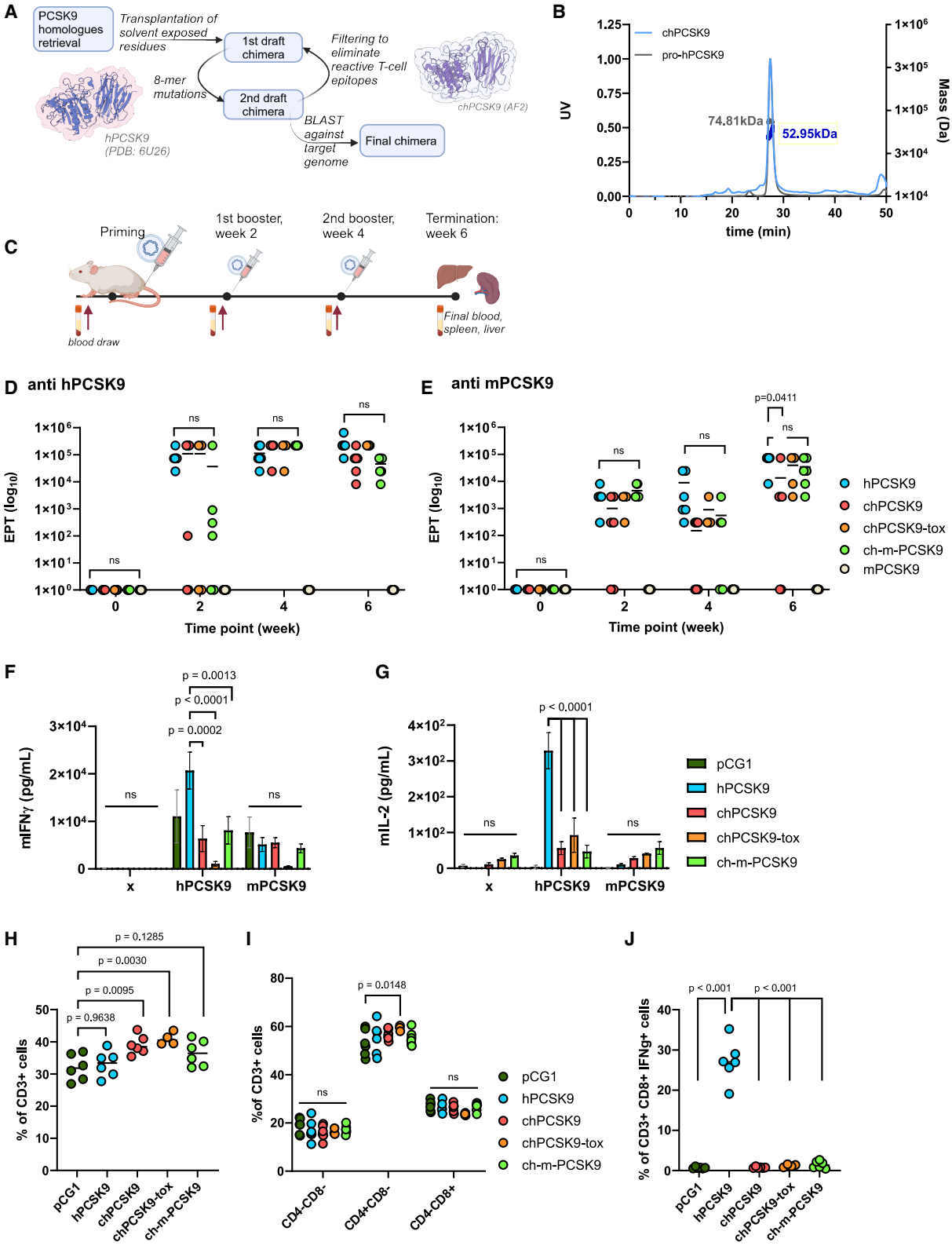


*(legend on next page)*

showed a good superposition of both chimeras with native PCSK9s, with the conformational surface epitopes largely conserved (Figures 1A and S1C). Greater variability was restricted to the unstructured linkers, connecting both lobes as well as segments inside the protein (Figures S1A and S1B).

Recombinant chPCSK9 was purified using NiNTA (Figure S2A). SEC-MALS analysis (Figure 1B) showed that the purified recombinant chPCSK9 is monomeric, with molar mass (52.9 kDa) and elution time, consistent with that of hPCSK9 (57 kDa mature chain; with bound prodomain 74.3 kDa). The CD spectra (Figure S2B) of chPCSK9 showed a pattern characteristic of the β-sheet curve, similar to hPCSK9, suggesting similar secondary structure. To provide an additional stimulus for immunization, we appended a universal $CD4^+$ T cell epitope, tetanus toxoid,[35,36] to the C-terminal end of chPCSK9, which acts as an adjuvant and further stimulates the maturation of PCSK9-specific antibody-producing B cells.[35,36]

### Immunization of BALB/c mice with chimeric PCSK9

The advantage of immunization with nucleic acids encoding protein antigens is that the same delivery platform is used for each construct, differing only in the sequence encoding protein antigens.[37] In addition to mRNA-based vaccines, plasmid DNA has also been used for vaccines, the main advantages being stability and low production costs.[34]

BALB/c mice were immunized with plasmid DNA encoding target sequences (mPCSK9, hPCSK9, chPCSK9, chPCSK9-tox, chmPCSK9, and an empty vector, pCG1 as a control; Figure S2C). Immunization of mice with DNA plasmids in three doses (priming, followed by two boosters) resulted in the formation of antibodies against hPCSK9 or mPCSK9 (Figures 1D and 1E). The highest mean endpoint titers (EPTs) of antibodies against hPCSK9 were achieved after the full immunization schedule in all immunization groups except the mPCSK9 group (Figure 1D). This was expected as it was previously reported that syngeneic immunization does not induce specific antibodies against the target antigen without adding additional adjuvants to the vaccine.[38] When analyzing the antibody response to recombinant mPCSK9 protein (Figure 1E), we observed an overall higher EPTs compared to hPCSK9 EPT. The highest EPTs were achieved after a full immunization regimen. In the case of the human-based chimeric construct (chPCSK9; red dots), one of the mice did not respond to immunization (no significant EPT was observed), and there was also no response to syngeneic immunization.

To determine the safety of a chimeric autologous vaccine, we investigated T cell cytotoxicity by isolating and analyzing mouse splenocytes and their response to recombinant proteins. Splenocytes' populations were analyzed by flow cytometry and stimulated with recombinant hPCSK9 and mPCSK9 to determine whether vaccination elicited a PCSK9-specific T cell response. Splenocytes in the hPCSK9-vaccinated group produced significantly higher levels of interferon gamma (IFNγ) and interleukin-2 (IL-2) compared to the other groups (Figures 1F and 1G), suggesting that elimination of T cell epitopes in chimeric sequences, reactive to hPCSK9, was functioning.

Analysis of splenocyte cellular subtypes by flow cytometry showed no statistically significant differences in the presence of T cells ($CD3^+$ cells), except in the chPCSK9-tox-vaccinated group compared to the control and hPCSK9 groups (Figure 1H). Similarly, when $CD3^+$ subtypes were analyzed for the $CD4^+$ helper T cells, the difference between the amount of T-helper cells in the chPCSK9-tox group compared to control was found as statistically significant (Figure 1I; panel $CD4^+CD8^-$), while in other subtypes (naive T cells, CTLs), there were no significant differences between the immunization groups (Figure 1H; panels $CD4^-CD8^-$, $CD4^-CD8^+$). In the nonstimulated CTLs ($CD4^-CD8^+$), we observed that the number of IFNγ-producing cells ($CD4^-CD8^+IFN\gamma^+$) differed significantly

**Figure 1. PCSK9 chimera design process with protein characterization and proof-of-concept BALB/c immunization, with serum endpoint titers and splenocyte (T cell) reaction assay**

(A) The algorithm, showing the design process to determine chimera sequence, the chimera model (chPCSK9), and the model of the mature hPCSK9 chain (PDB: 6U26). (B) SEC-MALS of purified recombinant human (hPCSK9, gray) and chimeric human (chPCSK9, blue) proteins, exhibiting the molar mass (74.81 kDa for hPCSK9 and 52.95 kDa for chPCSK9) and protein integrity (single peak). hPCSK9 is present with the bound prodomain, whereas chPCSK9 consists only of the mature chain. (C) The diagram of the vaccination regime shows three consecutive injections: priming, followed by two boosters 2 weeks apart. The relevant organs (spleen, liver, muscles) were harvested with the final blood. (D) Endpoint titers of total IgG antibodies against hPCSK9, determined by ELISA. The overall statistical significance for each time point was calculated using a two-way ordinary ANOVA, comparing all immunization groups to hPCSK9 group. Each immunization group is shown separately (hPCSK9: blue, chPCSK9: red, chPCSK9-tox: orange, chmPCSK9 (chimeric mouse): green, mPCSK9 (mouse): beige); individual dots represent each animal within the immunization group. $n = 6$ for all immunization groups except for chPCSK9-tox, where $n = 4$. (E) Endpoint titers of total IgG antibodies against mPCSK9, determined by ELISA. The overall statistical significance for each time point was calculated using a two-way ordinary ANOVA, comparing all immunization groups to hPCSK9 group. Each immunization group is shown separately (hPCSK9: blue, chPCSK9: red, chPCSK9-tox: orange, chmPCSK9: green, mPCSK9: beige); individual dots represent each animal within the immunization group. $n = 6$ for all immunization groups except for chPCSK9-tox, where $n = 4$. (F and G) ELISA showing quantification of mIFNγ (E) and mIL-2 (F) released from isolated splenocytes upon stimulation with 50 μg/mL recombinant hPCSK9 or mPCSK9, indicated on the *x* axis. Significance was calculated using an ordinary two-way ANOVA; results are shown as mean ± SEM of each immunization group, colored same as in Figure 1D. (H) Unstimulated (fresh) splenocyte flow cytometry analysis, showing the presence of $CD3^+$ T cells in each immunization group (colored as in Figures 1D and 1E). Significance was calculated using ordinary one-way ANOVA. Each dot represents each animal within the immunization group. (I) Unstimulated splenocyte flow cytometry analysis of T cell subsets on the *x* axis (naive $CD4^-CD8^-$, T helper cells $CD4^+CD8^-$, cytotoxic T cells $CD4^-CD8^+$) in each immunization group (colored as in Figures 1D and 1E). The statistical significance was calculated using ordinary one-way ANOVA. Each dot represents each animal within the immunization group. (J) Unstimulated (fresh) splenocyte flow cytometry analysis of $IFN\gamma^+$ $CD8^+$ T cells in each immunization group (colored as in Figures 1D and 1E). Significance was calculated using an ordinary two-way ANOVA. Each dot represents each animal within the immunization group.

**Table 1. MHC class I 8-mer binders for chPCSK9 and hPCSK9**

| Protein | MHC class I binding peptide (8mer) | MHC class I supertypes | Strength |
|---|---|---|---|
| chPCSK9 | TPNVVAAM | HLA-A2601, HLA-B0702 | weak |
| hPCSK9 | **HVAGIAAM** | HLA-A2601, HLA-B3901 | **strong** |
| | **SMRSLRVL** | HLA-B0801 | **strong** |
| | **YAIARCCL** | HLA-B0801 | **strong** |
| | LPGTSHVL | HLA-B0801, HLA-B3901 | weak |
| | TPNLVAAL | HLA-B0702, HLA-B3901 | weak |
| | TSHVLGAY | HLA-A0101, HLA-A2601 | weak |

**Table 2. MHC class I strong binders for chmPCSK9 and mPCSK9**

| Protein | MHC class I binding peptide (8-mer) | H2 allele (MHC I) |
|---|---|---|
| chmPCSK9 | TVTDFSSV | H-2-Kb |
| | SEPEVLTV | H-2Kq |
| | HETGGELL | H2-Kk, H2-Kq |
| mPCSK9 | SAPEVITV | H-2-Dd |
| | TITDFNSV | H-2-Kb |
| | VYLLDTSI | H-2-Kd |
| | HETGGQLL | H-2-Kk |
| | QPVTLGTL | H-2Lq, H-2-Ld |

from the other groups (Figure 1J). While hPCSK9 immunization resulted in the highest number of hPCSK9-reactive T cells (Figures 1H–1J), elimination of PCSK9-specific T cell epitopes in the chimeras strongly diminished the potential cytotoxicity while maintaining the formation of PCSK9-specific antibodies.

### Long-term immunization study in an ApoE$^{-/-}$ atherosclerosis model

This work aimed to explore the potential of vaccination as a therapy for atherosclerosis. Therefore, we wanted to test the chPCSK9 vaccine in an atherosclerosis mouse model to evaluate its long-term effects. We used an atherosclerosis mouse model with knocked-out apolipoprotein E (ApoE$^{-/-}$) in which atherosclerotic plaques recurrently develop due to poor clearance of cholesterol-bound lipoproteins.[39–41] The ApoE is the main component of chylomicrons and very-low-density lipoprotein (VLDL) particles, and its deficiency leads to an overall increase in total plasma cholesterol level (TC).[39,40,42] These mice have a 5-fold increase in TC levels compared to wild-type mice fed a standard chow diet (wt: 101–119 mg/dL; ApoE$^{-/-}$: 360–885 mg/dL),[40,41,43] making the mouse model capable of developing severe atherosclerosis symptoms, including macrophage infiltration to foam cell formation, plaques, and fatty streaks.[39,44]

The immunization regime was the same as for the proof-of-concept BALB/c immunization, except that the duration of the *in vivo* experiment was extended to observe the prophylactic effect of the chimeric vaccine on atherosclerosis pathogenesis (Figure 2A). Again, we quantified the immunoglobulin G (IgG) endpoint titers[45] of the antibodies produced, which are cross-reactive against both hPCSK9 (Figure 2B) and mPCSK9 (Figure 2C). The majority of mice ($n = 5$) reached a plateau for hPCSK9 at week 9, which persisted until week 18 when the EPT began to fall. For mPCSK9, EPTs are more scattered from the second booster (blood collection in week 6) until the end of the experiment; however, EPT is higher compared to hPCSK9-specific EPT at week 24.

We then quantified the total serum mPCSK9 (Figure 2D), triglycerides (Figure 2E), and the serum cholesterol (Figures 2F, 2G, and S4A). In the control group (pCG1) the serum mPCSK9 levels steadily increased until the end of the experiment, which is consistent with previous reports showing a positive correlation between increasing age and PCSK9 level.[46] In the chPCSK9-tox group, the highest concentration was reached after the first booster (week 4) but was not found as significantly different from the control group at that time point. After week 4 until the end of the experiment, the mPCSK9 concentration remained stable and was at the end of the experiment significantly lower than in the control group. Serum triglycerides (Figure 2E) were quantified at the beginning of the experiment (t = 0), at full vaccination regime (t = 6), and at the end of the experiment (t = 24). While the first two time points are not statistically significant, the average values after full vaccination regime and at the end of the experiment indicate a reduction in triglyceride levels. Levels of total cholesterol (TC), cholesterol esters, and free cholesterol were quantified at each blood sampling time point to assess the efficacy of the vaccine in lowering cholesterol levels. We observed a significant decrease in TC levels (Figure 2F) at week 15, which persisted until the end of the trial. For cholesterol esters (Figure 2G), the values of the control and chPCSK9-Tox groups overlapped until after the final time points

**Table 3. Predicted CTL epitopes for chPCSK9 and hPCSK9**

| Protein | CTL epitope | MHC class I supertypes |
|---|---|---|
| chPCSK9 | ASSECNTCF | A1, B58, B62 |
| | EVLQTMIHY | A1, A26, B62 |
| | IARAGAVVL | B7, B8, B62 |
| | SAAPGTSAL | B7, B39, B62 |
| | VLLPFIGGY | A1, A3, A26, B62 |
| | VVLAAAGNY | A1, A3, B62 |
| hPCSK9 | ALPGTSHVL | A2, B39, B62 |
| | ASSDCSTCF | A1, B58, B62 |
| | ELRQRLIHF | A26, B8, B62 |
| | GTSHVLGAY | A1, A3, A26, B62 |
| | HLAQASQEL | A2, B39, B62 |
| | LSAEPELTL | B39, B58, B62 |
| | LVCRAHNAF | B8, B58, B62 |
| | RLARAGVVL | B7, B8, B39, B58, B62 |
| | VLLPLAGGY | A1, A3, B62 |
| | YAVDNTCVV | A2, A26, B7, B39 |

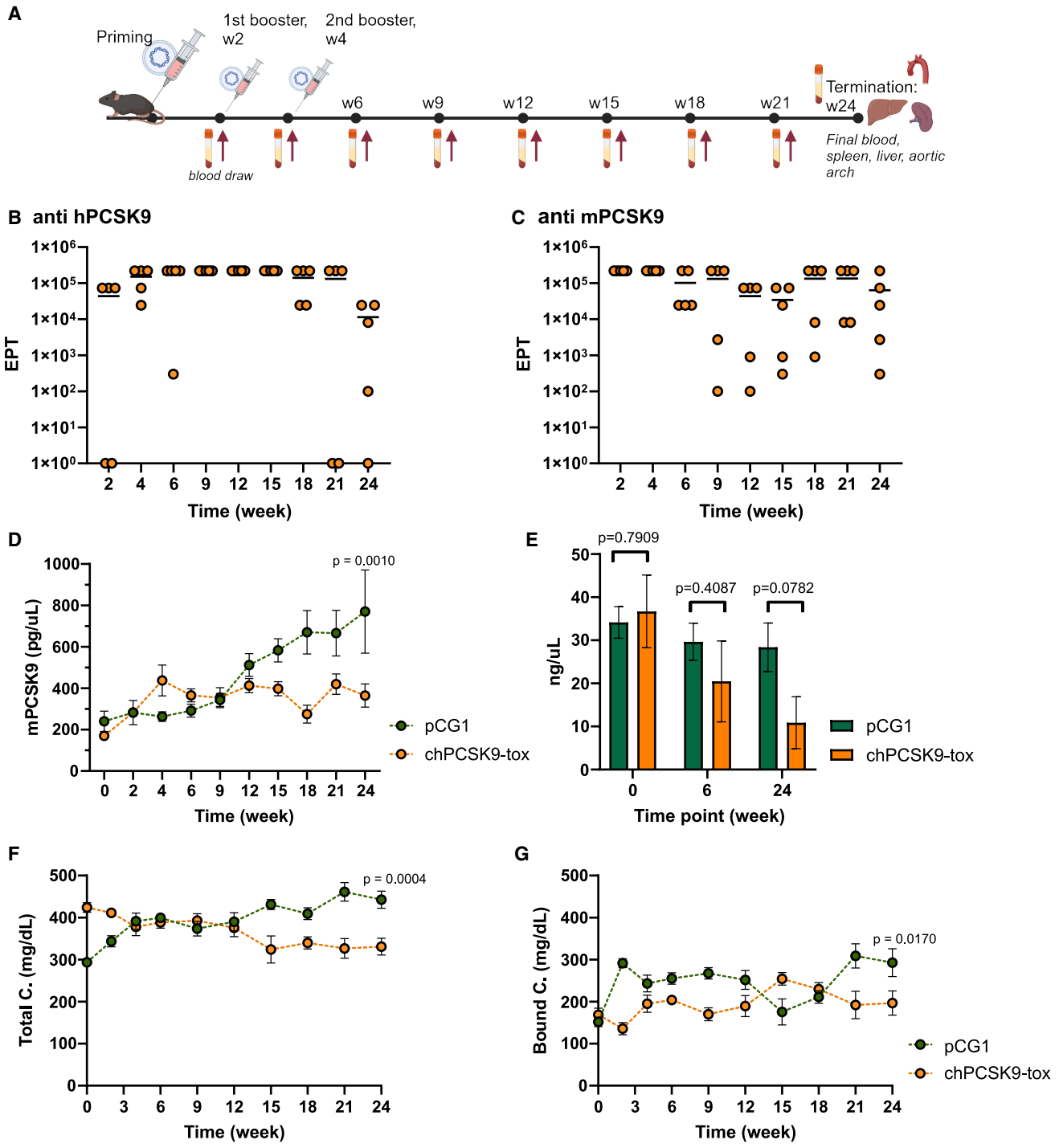


**Figure 2. Atherosclerosis model (ApoE$^{-/-}$ mice) immunization with serum analyzes (endpoint titer determination, mPCSK9 quantification, and total cholesterol quantification)**

(A) The diagram of the vaccination scheme for ApoE−/− mice shows three consecutive injections, each 2 weeks apart (priming, two boosters). Blood was drawn before each injection; after week 6, blood samples were collected every 3 weeks until the experiment was terminated (week 24). Final blood and relevant organs (spleen, liver, aortic arch) were collected at end of the trial. $n = 5$ per immunization group (pCG1 and chPCSK9-tox). (B) Endpoint titers of total IgG antibodies against hPCSK9 determined by ELISA. Individual dots represent each animal within the immunization group ($n = 5$). (C) Endpoint titers of total IgG antibodies against mPCSK9 determined by ELISA. Individual dots represent each animal within the immunization group ($n = 5$). (D) Quantification of mPCSK9 over 24 weeks, determined by ELISA. Green dots show the amount of mPCSK9 at

*(legend continued on next page)*

at weeks 21 and 24. However, the differences between free cholesterol (Figure S4A) remained statistically insignificant throughout the trial.

### Vaccination increases liver LDLR and regulates lipid homeostasis in ApoE$^{-/-}$ mice

Cholesterol homeostasis is regulated by the liver, and the majority of PCSK9 is also produced and secreted by hepatocytes.[4] We analyzed LDLR and mPCSK9 in the liver tissue lysates to determine how chPCSK9 vaccination affects interaction of PCSK9 with hepatic LDLR (Figures 3A, S5A, and S5B). chPCSK9-tox-vaccinated mice retained higher levels of LDLR than those in the control group (Figure 3A), which was also observed in liver histology slides, stained with anti-LDLR antibodies (Figure 3B).

At the protein level, inhibition of PCSK9 achieved the desired effect (increased amount of LDLR on the hepatocyte plasma membrane), but we wondered whether vaccination could also affect the liver transcriptome. To assess the gene expression profile of the liver after chPCSK9-tox vaccination, RNA sequencing (RNA-seq) and RT-PCR of total liver mRNA were performed. Both methods revealed insignificant changes in the expression of both *Pcsk9* and *Ldlr* (Figures 3C, S5D, and S5E), indicating that the inhibition of PCSK9 occurs at the protein level and does not affect the gene expression of the two proteins.

However, we observed significant changes in the expression of several transcripts related to cholesterol and fatty acid metabolism and in redox/inflammation pathways[44] (Figures 3C–3E). The upregulated genes with log fold change (LFC) above 2 include liver-characteristic genes (such as cytochrome P450 polypeptides; Figure 3C), while the downregulated group consists of apolipoprotein-related genes and fatty-acid-binding proteins (a representative set is shown in Figure 3D). The inflammatory biomarkers (*Crp*, haptoglobin gene, *Saa* genes) and some of the immune response genes (*Ccl11*, *Ccr6*) were also significantly downregulated in chPCSK9-tox group (Figure 3D), suggesting a reduced inflammatory state of developing atherosclerosis. To exclude a possible autoreactive response against hepatocytes, we also measured markers for liver disease/inflammation in serum, which did not differ significantly from the control group (Figure S4B). *Fgf21* (fibroblast growth factor 21) and *Cd36* stand out among the identified upregulated genes. Both are regulated via activation of the PPAR pathway, with FGF21 playing a protective role[47–49] and CD36 being pro-atherogenic as it is involved in lipid accumulation and inflammatory signaling.[50,51] PCSK9 directly interacts with and inhibits CD36.[51,52] Therefore the inhibition of PCSK9 by vaccination may lead to an increase in CD36. The enriched pathways of all significantly upregulated genes (Figure 3E) are categorized into the KEGG pathways describing fatty acid degradation, cholesterol metabolism, and PPAR-related pathways (peroxisome and PPAR signaling pathway).

These results suggest a link between the anti-atherogenic effect of the chPCSK9 vaccine, a compensatory effect due to the reduced hepatic cholesterol levels, and a developing inflammatory state due to ApoE$^{-/-}$ phenotype.

### chPCSK9 vaccination suppressed atherosclerosis development in ApoE$^{-/-}$ mice

To determine the pathophysiological effect of the chimeric vaccine, we investigated atherosclerotic lesions and lipid accumulation in the aortas and adjacent tissue of immunized ApoE$^{-/-}$ mice. We found that both the pCG1 and chPCSK9-tox group had oil-red-o-stained (ORO-stained) areas, with pCG1 being substantially larger. The chPCSK9-tox immunization reduced the number of lipid plaques in the arterial walls and overall lipid accumulation in the adjacent tissues (Figure 4A), consistent with generally lower TC values in the mice sera. The ORO-stain sizes were widely distributed in the cross-sections of control group. They appeared both as fatty streaks in the arterial walls and as lipid droplets in the surrounding adipose tissue (Figure 4C). In the control group, more severe plaques formed, showing evidence of thickening of the aortic tunica intima (Figure 4C), whereas in the chPCSK9-tox group, arterial walls were thinner and fewer plaques occurred (Figures 4B and 4C).

In addition, a higher number of monocytes adhering to the inner vessel wall was observed in pCG1, and larger plaques with lipid core and inflammatory cells (foam cells and other macrophage-like infiltrated cells) were formed (Figures 4C and 4D). Mac-3 staining was present in the cellular accumulations on the aortic walls of the control group, in contrast to the vaccinated group, in which much weaker Mac-3 staining was observed (Figure 4D, red arrows). Thus, vaccination therefore substantially impaired atherosclerotic development *in vivo*, and the disease burden was significantly milder in the chPCSK9-tox-vaccinated animals.

## DISCUSSION

Several strategies for vaccination against autologous proteins such as PCSK9 have been investigated, from xenogeneic[38] to peptide vaccines[22,24] and presentation of PCSK9 epitopes on virus-like particles (VLPs).[23,25,26] Xenogeneic vaccination of mice with hPCSK9 was shown to be effective in reducing the major risk factor for

a specific time point (*x* axis) in the control group, pCG1. Orange dots are the mPCSK9 levels of the chPCSK9-tox group. Results are shown as mean ± SEM; significance at the termination of experiment, *p* value, was calculated using ordinary two-way ANOVA. (E) Quantification of triglycerides at the time points 0, 6, and 24 weeks (*x* axis; start of the experiment, complete immunization, and end of the experiment). Results are expressed as mean ± SEM, and significance (*p* value) was calculated by t test comparing control pCG1 with chPCSK9-tox. (F) Cholesterol quantification shows total cholesterol levels at specific time points (*x* axis). Green dots represent the cholesterol levels of the control group, pCG1; orange dots are the cholesterol values of chPCSK9-tox. Results are expressed as mean ± SEM, and significance at the end of the experiment, *p* value, was calculated using ordinary two-way ANOVA. (G) Quantification of cholesteryl esters is shown at each time point of the two immunization groups (pCG1 [control], green and chPCSK9-tox, orange dots). Results are expressed as mean ± SEM, significance at the end of the experiment, *p* value, was calculated using ordinary two-way ANOVA.

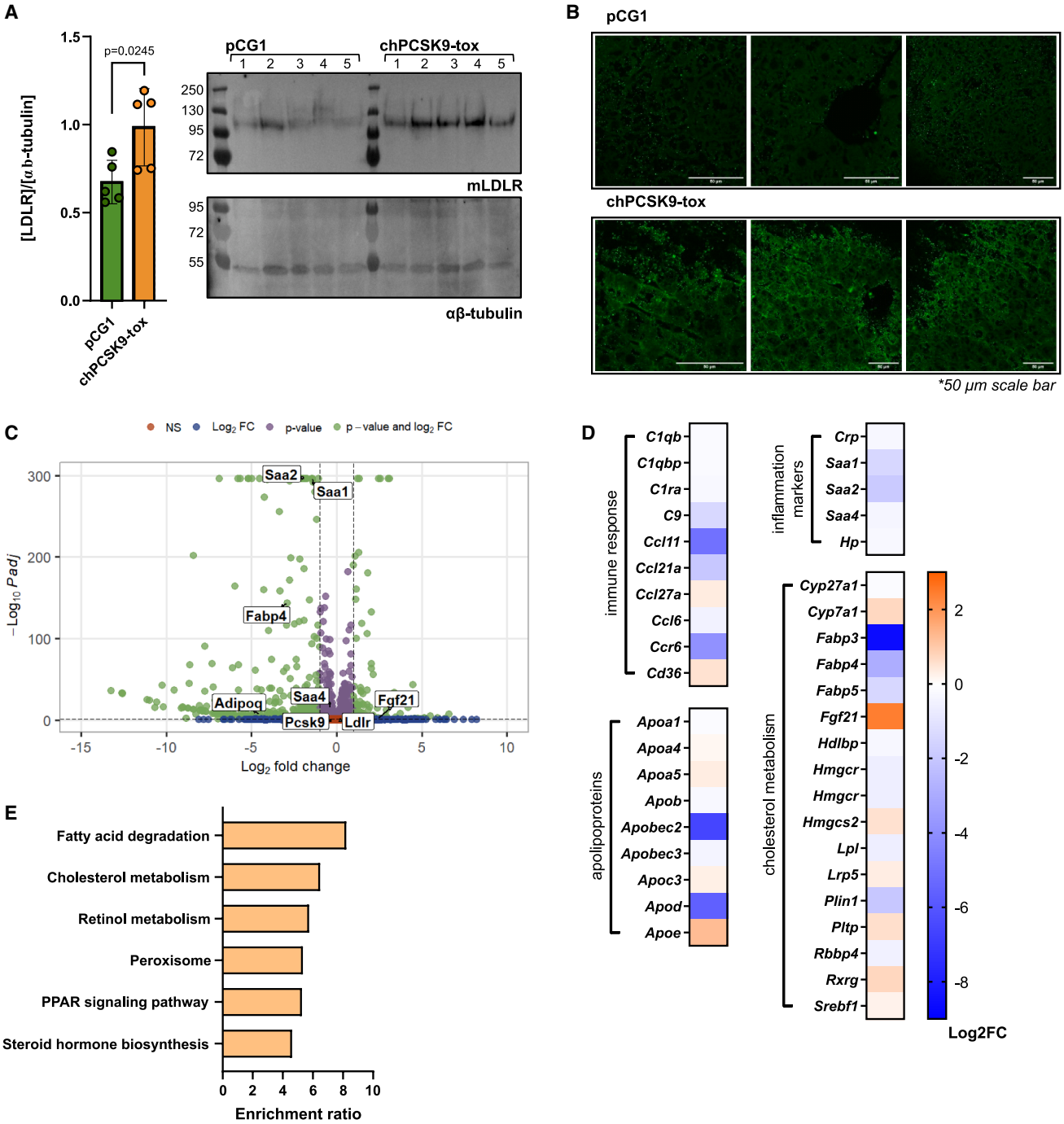


**Figure 3. Analysis of lipid homeostasis in the liver of ApoE–/– mice, including expression of LDLR and assessment of the liver transcriptome**

(A) Relative quantification (left) of mLDLR in liver tissue lysates was determined by immunodetection of proteins on nitrocellulose membrane (right). The upper membrane shows mLDLR expression at 100 kDa in each animal (5) of the control (pCG1) and chPCSK9-tox immunization groups. The bottom membrane shows the loading control—(αβ-tubulin) at 55 kDa. The complete membranes are shown in Figure S5A. The relative amount of mLDLR (left graph) was quantified with ImageJ and is normalized with the loading control (αβ-tubulin). The green column is the control group, and the orange column is the chPCSK9-tox group. Results are presented as mean ± SEM; significance was calculated using an unpaired t test. (B) Representative images of cross-sections of paraffin-embedded liver tissue (confocal microscopy, 50 μm scale bars). The top three images are from the control group and the bottom three are from chPCSK9-tox group. (C) Enhanced volcano plot, showing the results of the analysis of the liver RNA-seq, using the R package DESeq2. Each point represents a gene, positioned in the graph according to its expression (LFC, *x* axis) and the significance of its expression ($p_{adj}$,

*(legend continued on next page)*

atherosclerosis: high serum cholesterol. However, the potential risk of autoimmunity was not investigated in that particular study. The follow-up studies addressed this question, using different variants of epitope vaccines that used only short AA sequences of hPCSK9 instead of the whole cognate protein. For example, a VLP vaccine with linear epitopes of hPCSK9, interacting with LDLR, elicited a PCSK9-specific antibody response and led to a decrease in key lipid parameters in macaques.[23] In another study, different hPCSK9 epitopes associated with LDLR binding were used, with a focus on B cell activation.[24] By analyzing and selecting eight AA long human B cell epitopes, the authors of the study were able to avoid potential T-cell-related tissue damage.[24] The most promising vaccine both covering PCSK9 neutralization and overcoming humoral and cellular autoimmunity used the AFFITOPE technology, in which short peptides resembling the native homologs were used as PCSK9-specific antibody-inducing epitopes.[22] However, this approach cannot generate discontinuous conformational epitopes[27,53] that are typically required for high-affinity antibodies and/or elicit polyclonal antibody response. On the other hand, a study[54] comparing peptides with the full-length PCSK9, conjugated to VLPs, showed lower efficacy of the full-length vaccine, underlining the superiority of peptide VLP vaccines compared to protein VLP vaccines.

We have presented a proof-of-concept approach for vaccine development in which a native (autologous) target is modified by a "deimmunization" algorithm. *We investigated whether B cell tolerance-breaking immune response could be induced with chPCSK9 that maintains the same conformational epitopes, preventing the development of atherosclerosis without triggering the cytotoxic T cell response.* Structural models of a thoroughly reconstructed chimeric PCSK9 sequence indicate that they have similar global folds as the native ones. Compared to the human homolog, which contains several 8-mer or 9-mer peptides, that can bind at least three different HLA molecules, the chPCSK9 sequence has a much lower "$CD8^+$ T cell activating" propensity. We observed that splenocytes from chimera-vaccinated mice reduced the production of cytotoxic T cell cytokines compared to strong reactivity against hPCSK9, suggesting that this type of vaccine is indeed safer in terms of autoimmune reactivity 2 weeks after full immunization regime. However, while the analyses of endpoint titers represent longitudinal analysis of B cell reactivity, *in vitro* stimulation of T cells with recombinant proteins shows a response at a specific time point. Additional preclinical *in vivo* studies would allow an accurate assessment of T cell kinetics and T-cell-based autoimmune reactivity in vaccination against endogenous targets.

The suppression of atherosclerosis development was shown to last for 24 weeks, both in the liver and in the aortic arches. The inflammatory state, characteristic for atherosclerosis, was improved in the chPCSK9-vaccinated mice compared to the pCG1 group, while we observed a compensatory effect in the liver transcriptome due to the inhibition of PCSK9 and lowered TC. In addition to the DNA-plasmid-based vaccination used here, the chimeric protein vaccine could also be administered using mRNA/LNP or in the form of a protein vaccine. Both methods have shown to be safe and effective platforms for vaccine delivery and might elicit an even stronger humoral immune response.[55] DNA vaccines may also carry a potential risk of insertional mutagenesis, which can be avoided with mRNA or protein-based vaccines.

The recent development of machine-learning-based protein design (ProteinMPNN,[56] RF diffusion,[57] FoldingDiff[58]) facilitates the design of protein backbones with increased stability and selection of conserved residues that could be used for the construction of protein vaccines,[59,60] combined with the elimination of MHC class I epitopes (CTL epitopes) against the endogenous proteins as shown in a recent preprint.[61] Despite the ability to completely remodel the core of proteins as vaccines, conservation of residues based on homologs (similar to the selection of a distant homolog here) nevertheless increased the success rate of preserving the protein fold and functionality.[56] T-cell-reactive peptide prediction software was human-based at the time of chimera development, so mouse models were less suitable for predicting effects on autoimmune reactivity. Nevertheless, we have developed and tested a vaccine that can produce antibodies that can bind to autologous targets *in vivo*. Although the use of mouse models in atherosclerosis research may have limited applicability to humans (differences in lipid profile, site of lesions development, etc.),[62,63] we chose $ApoE^{-/-}$ mice because our proof-of-concept vaccine is based on the prevention of the interaction of PCSK9 with LDLR. The vaccination therefore produced the desired effect to some extent: by lowering TC and mPCSK9 serum levels, it suppressed the development of atherosclerotic symptoms in a mouse model prone to develop atherosclerosis. The potential advantages of DNA-based platform are lower frequency of immunization and better affordability due to lower costs of manufacture compared to monoclonal antibodies or synthetic RNA. Furthermore, using full-length proteins could elicit polyclonal antibody response, attacking same target (PCSK9) at different sites.

While several recent platforms have emerged to modify the genomic PCSK9 by base editors[64] or epigenetic suppression of PCSK9 expression,[65] the vaccination is a well-established and safe therapy that complements to the already proven and safe antibody-based therapy. An

*y* axis). The graph shows 2,037 differentially expressed genes ($p_{adj.} < 0.05$), above the dotted line. Red dots are genes with insignificant expression; blue are insignificant ($p_{adj.} > 0.05$) that are upregulated (LFC >1; right side) or downregulated genes (LFC < −1; left side). Significantly expressed genes ($p_{adj.} < 0.05$) are purple (−1 < LFC <1) and green (upregulated, right side; downregulated, left side). Genes, relevant to the study, are specifically labeled. (D) Heatmaps showing the differential expression of significantly upregulated (red) and downregulated (blue) genes, determined with the R package DESeq2. Genes are grouped into panels, according to their role: immune response genes, apolipoproteins, inflammation markers, and genes, related to cholesterol metabolism. (E) Overrepresentation analysis of significantly upregulated genes ($p_{adj.}$ <0.05, LFC >0). The gene sets of the enriched metabolic pathways were categorized using the KEGG database (*y* axis), and the enrichment ratio was calculated using the WebGestalt tool available online.

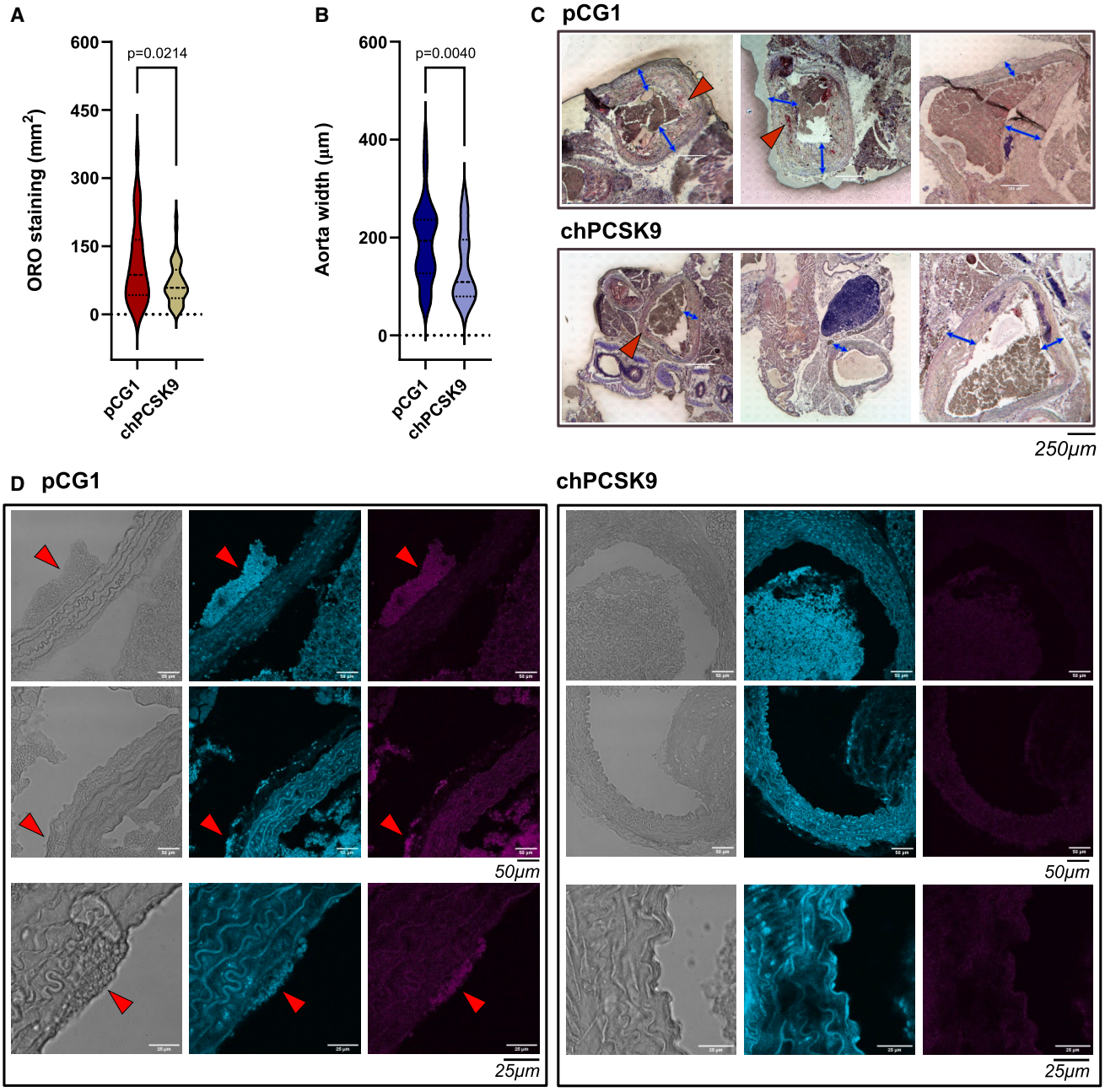


**Figure 4. Atherosclerosis development in aortic arches and adjacent tissues of ApoE–/– mice, vaccinated with human chimeric PCSK9 (chPCSK9-tox)**
(A) Violin plot of ORO staining area results of aortic arch histology slides, obtained using the deconvolution approach in ImageJ. The red data represent control group; the yellow data represent chPCK9-tox. Significance was calculated using the unpaired Welch's t test. (B) Aortic widths of the aortic arch histology slides, measured in ImageJ with the measuring tool. The dark blue data represents the control group; the light blue data represent the chPCK9-tox group. Significance was calculated using the unpaired t test. (C) Representative micrographs of the aortic arch of control (pCG1) and chPCSK9-tox groups. Red arrows show ORO-stained areas, and blue arrows show representative width measurements. The scale used for all images is 250 µm. (D) Representative confocal microscopy images of aortic walls, showing presence of Mac-3 (CD107b; magenta) with Hoechst 33342 (cyan) as counterstain for the nuclei. The scale used is 50 µm for the first two rows and 25 µm for the last row. Pink arrows indicate developing atherosclerotic plaques on the aortic walls.

important aspect to consider for vaccines against endogenous targets is the risk ratio for patients receiving such a vaccine. The established strategies (e.g., monoclonal antibodies) to ameliorate atherosclerosis show a significant reduction in cardiovascular events, and for (PCSK9)-based vaccines the hazard ratio achieved should be comparable or better than for these existing therapies. While the evaluation of the hazard ratio can be accurately determined by a clinical study, additional preclinical studies in non-human primates (as some recent VLP-based PCSK9 vaccine studies have shown[25,26]) should provide an estimate of the hazard ratio and could clarify the efficacy of this platform and its suitability for use in humans due to the differences between mice and humans. They could also provide information on the long-term persistence of antibodies, the response to repeated booster vaccinations, and additional data on autoimmunity risks such as epitope spreading and antibody-dependent cellular cytotoxicity.

## MATERIALS AND METHODS

### Design and molecular modeling of chimeric PCSK9

We retrieved the protein sequences of PCSK9 homologs from the Uniprot database[66] and the determined percentage of homology, using the Clustal Omega alignment engine.[67] The first draft of chimeric PCSK9 was obtained by transferring solvent-accessible amino acids (30% SAS determined using the UCSF Chimera molecular modeling system[68,69]) from native (human and mouse) protein to a chosen distant homolog of PCSK9 (*Mola mola*). Regions with more than eight AA matching the native homologs were disrupted with minimally invasive AA mutations. Subsequently, the chimera designs and the native sequences were used as inputs to the online tools NetMHC-4.0,[30] NetCTL-1.2 tool,[31] and NetH2Pan[32] to search for peptides that can bind MHC class I molecules, focusing on 8-mer candidates. The threshold for strong binding was set to the default value (0.5% rank) and for weak binding to 2%. The 8-mer peptides found were mutated again. Several intermediate draft sequences were obtained, which were subjected to an iterative process of epitope prediction and subsequent AA mutation. The final chimeric sequences were used for homology modeling with AlphaFold2[33,70] and AlphaFold3.[34]

### Cloning and plasmids

All DNA constructs were prepared using conventional cloning methods (Gibson assembly), based on synthetic DNA (Twist, San Francisco, CA, USA) or ordered from Addgene. pAAV/D374Y-hPCSK9 was a gift from Jacob Bentzon (#58379; http://n2t.net/addgene:58379; RRID:Addgene_58379),[71] pcDNA3.1-mPCSK9 from Liming Pei (#122678; http://n2t.net/addgene:122678; RRID:Addgene_122678),[72] and pBa-LSS-GFP-LDLR wt from Gary Banker and Marvin Bentley (#98184; http://n2t.net/addgene:98184; RRID:Addgene_98184).[73] All constructs, including chPCSK9, were codon optimized and cloned into the pCG1 expression vector, which was a gift from Stefan Pöhlmann (German Primate Center––Germany; SARS-CoV-2 pCG1-S and human ACE2 pCG1-hACE2).[74]

### Production and characterization of proteins in Expi293F cells

Expi293F cells (Thermo Fisher) were cultured in Expi293 expression medium (Thermo Fisher) at 37°C and 8% $CO_2$ on an orbital shaking platform. Cells were transfected using the ExpiFectamine 293 Transfection Kit according to the manufacturer's instructions. Supernatants, containing protein samples, were filtered through 0.2 μM filter units (Sartorius) and then purified on NiNTA resin (Golden Biotechnology, St Louis, MO, USA), previously equilibrated with NiNTA A buffer (20 mM Tris at pH 7.5, 10 mM imidazole, 150 mM NaCl, 1 mM TCEP, pH 7.5). After washing with 20 mM imidazole, the bound proteins were eluted with 300 mM imidazole, characterized by SDS-PAGE, and pooled and dialyzed overnight in PBS. Proteins were concentrated to 1 mg/mL, snap-frozen in liquid nitrogen, and stored at −80°C. Circular dichroism (CD) measurements were performed using the Chirascan CD spectrometer (Applied Photophysics). Proteins were dialyzed overnight against 100 mM KF, 10 mM KH2PO4 at pH 7.5, and concentrated to 0.2 to 0.3 mg/mL prior to the measurement. Protein spectra were recorded in far-UV (190–350 nm) at 20°C, 1 nm step, 1 nm bandwidth, and a scan time of 1 s in a 1-mm quartz cuvette (Hellma). Size exclusion, coupled with multi-angle light scattering (SEC-MALS), was performed using HPLC system (Waters) with UV- (Waters), Dawn8+ MALS- (Wyatt), and RI-detectors (Shodex). Samples were concentrated to 0.7 mg/mL (Millipore, Merck), filtered through 0.1 μM centrifugal filters (Millex, Sigma-Aldrich), and injected onto Superdex200 Increase 10/300 column (Cytiva, Marlborough, MA, USA), equilibrated with 20 mM Tris, 150 mM NaCl, pH 7.5, and 1 mM TCEP. The data were analyzed with Astra 7.0.

### Immunization of animals

The immunogenicity of the vaccine was tested in female 8- to 10-week-old mice, BALB/c OlaHsd mice (Envigo, Desio MB), and $ApoE^{-/-}$ mice (strain B6.129P2-Apoetm1Unc/J; Charles River). All animal experiments were approved by the Administration of the Republic of Slovenia for Food Safety, Veterinary and Plant Protection of the Ministry of Agriculture, Forestry and Foods, and Republic of Slovenia (Permit number U34401-26/2021/5) and conducted in accordance with EU directive 2010/63. The mice were kept in a 12–12 h dark-light cycle at 40%–60% relative humidity and a room temperature of 20°C–24°C. The laboratory animals were housed in individually ventilated cages (IVCs) (Techniplast) and fed with standard chow (Mucedola); tap water was provided *ad libitum*. All animals used for the study were healthy and had a health certificate from the animal vendor. The health/microbiological status was confirmed by the Mouse Vivum immunocompetent panel (QM Diagnostics) recommended by FELASA. Vaccination was carried out under general inhalation (1.8% MAK isoflurane anesthesia [Harvard Apparatus, Holliston]). Unless otherwise, each vaccination group contained six mice that were vaccinated three times according to the vaccination regime: priming, followed by two booster immunizations, each 2 weeks apart. The animals were vaccinated with plasmid DNA (empty pCG1 vector, hPCSK9, chPCSK9, chPCSK9-tox, chmPCSK9, mPCSK9), complexed with the *in vivo* transfection reagent jetPEI (Polyplus Transfection); N/P ratio was 12. Each animal received 20 μg of DNA plasmid via intramuscular injection with 30 G needle (Beckton Dickinson) into *m. tibialis anterior* after appropriate preparation of the area. With transfection reagent, the

amount was 50 μL per animal. One day before each vaccination, blood was taken from the lateral vein using the Microvette 300 (Sarstedt). Two weeks after the last boost in the BALB/c groups, the experiment was terminated and the animals were sacrificed. In the ApoE$^{-/-}$ groups, the experiment was terminated 24 weeks after the priming. We took final blood, spleens, liver, muscle tissue, and aortic arches with neighboring tissue. Mouse sera were prepared by centrifuging the blood samples at 3,000 rpm (20 min, 4°C). Liver samples used for qPCR/RNA-seq were frozen in liquid nitrogen, and liver samples and aortic arch samples for microscopy were placed in 10% neutral buffered formalin (Sigma Aldrich) until further analysis. ELISA was used for the EPTs. In-house produced recombinant hPCSK9 and mPCSK9 were coated on high-binding half-well plates (Greiner) in PBS buffer (Gibco) at 50 ng/well. Serial dilutions of mouse sera were added to plates (initially 1:100, followed by 3-fold dilutions). Horseradish peroxidase (HRP)-conjugated secondary antibodies for the determination of total IgG were added (goat anti-mouse IgG (H + L)-HRP, Jackson ImmunoResearch, 115-035-003). The color change of the substrate (TMB) was measured as absorbance at 450 and 620 nm using the SynergyMx multiplate reader (BioTek). Endpoint titers were determined as the highest dilution above the cutoff value, determined from the control group absorbance data.[45] Representative samples of muscle tissue were taken a day after vaccination to determine construct protein expression. Muscle tissue lysates were prepared with RIPA lysis buffer (10 mM Tris-HCL at pH 7.5, 100 mM NaCl, 10 mM EDTA, 0.5% Triton X-100, 0.5% NaDOC, 1 mM PMSF). Total protein concentrations in the samples were quantified with the BCA assay.

### Quantification of serum lipids, serum mPCSK9, and liver proteins

Total, bound, and free cholesterol of mouse sera were quantified using biochemical kits for cholesterol quantitation according to the manufacturer's instructions. (Amplex Red Cholesterol Assay Kit, Invitrogen, Thermo Fisher Scientific). Serum triglycerides were quantified according to manufacturer's instructions using Triglyceride Quantification Colorimetric/Fluorometric Kit (MAK266, Sigma Aldrich).Sera were also analyzed using a VetScan Mammalian Liver Profile (Abaxis) with a VetScan VS2 analyzer (Abaxis) according to the manufacturer's instructions. The amount of PCSK9 in mouse sera was quantified using the PCSK9 ELISA kit (SEK50251, Sino Biological) according to the manufacturer's instructions. Liver tissue lysates were prepared with RIPA lysis buffer (10 mM Tris-HCL at pH 7.5, 100 mM NaCl, 10 mM EDTA, 0.5% Triton X-100, 0.5% NaDOC, 1 mM PMSF). The protein concentrations in the samples were quantified with the BCA assay. Two hundred microgram per sample was used for SDS-PAGE under denaturing conditions, subsequently transferred to nitrocellulose membranes (Hybond ECL, GE Healthcare). Anti-LDLR (Sino Biological, cat. no. 50305-R032, clone 032) and anti-PCSK9 antibodies (Cell Signaling, cat. no. 85813S, clone D7U6L) were used for the quantification of the respective proteins; anti αβ-tubulin antibodies (Cell Signaling, Cat. No. 2148, polyclonal) were used as loading control. Membrane stripping was performed with membrane stripping buffer (6 mL 10% SDS, 21 μL β-mercaptoethanol, 2 mL TRIS pH 7.5, 25 mL MQ; 30 min, 50°C). Membranes were incubated with SuperSignal West Pico substrate (Thermo Fisher), and proteins were visualized on G-box (Syngene). Relative expression was quantified using ImageJ (Fiji)[75] according to the pixel quantification method by Hossein Davarinejad, available online. Briefly, we measured the mean gray values of the regions of interest (ROIs; selected protein bands of mLDLR, mPCSK9, and αβ-tubulin). Same frame was used for each protein band across a row. The final quantification values were determined as the ratio between the protein band of a given sample and the loading control of the same sample.

### Transcriptome analyzes

Total RNA was extracted from homogenized liver tissue using TriPure Isolation Reagent (Merck) and High Pure RNA Isolation Kit (Roche) according to the manufacturers' instructions. Quantity and purity were measured using Nanodrop spectrophotometer (Thermo Fisher). cDNA was reverse transcribed from 1 μg of RNA using a High-Capacity cDNA Reverse Transcription Kit (Applied Biosystems). qPCR was performed with the SYBR green I Master Kit (Roche) with the LightCycler480 instrument (Roche). The primers used are in the supplement (Table S1). Results are presented as the second derivative (ddCt) of the quantification cycle (Ct), relative to the house-keeping gene *Gapdh*.

For RNA-seq, four technical replicates were pooled by adding equal amounts of RNA to the sample mixture for both the pCG1 and the chPCSK9-tox groups. Azenta Life Sciences (Genewiz, Leipzig, Germany) performed sample quality control, library preparation, and rRNA removal by polyA selection for the mRNA species. Libraries were run on Illumina NovaSeq, using a 2 × 150 bp paired-end sequencing protocol with sequencing depth of 20–30 million reads per sample. The data were first trimmed using CutAdapt[76] within the RNAlysis software[77] (paired-end adapter trimming). Then, the trimmed samples were aligned to the mouse genome using the Kallisto pseudo alignment[78] (pre-produced index and gtf files were downloaded from the Kallisto transcriptome indices data source [version June 22 2019; kallisto 0.45.1, Ensembl v96 transcriptomes, https://github.com/pachterlab/kallisto-transcriptome-indices/releases; accessed Oct 19 2023]). Differential expression was performed using RStudio (RStudio 4.3.2 [2023-10-31 ucrt]) with the R package DESeq2.[79] Data were normalized using the built in function (median-of-ratios), and the significance threshold was set to the adjusted $p$ value <0.05. The volcano plot was drawn with Bioconductor package EnhancedVolcano.[80] Other graphs were drawn using GraphPad Prism 8. We used significantly upregulated genes ($p_{adj} < 0.1$; $\log_2FC > 0.5$) in the online-available WEB-based Gene Set Analysis toolkit (WebGestalt)[81] to perform overrepresentation analysis.

### Histology of the liver

After overnight fixation in 10% neutral buffered formalin (Sigma Aldrich) and subsequent storage in 70% ethanol, the samples were subjected to gradient ethanol dehydration and embedded in paraffin

(Leica Paraplast). The paraffin blocks were cut to 7 μm thickness using the rotation microtome RM 2245 (Leica), mounted on adhesive-coated slides (Leica Microsystems), and stored at room temperature. After deparaffinization and rehydration, tissues were immersed in pre-warmed antigen retrieval solution (10 mM citric acid at pH 6.0, 0.05% Tween 20). Samples were blocked with 3% BSA in DPBS and incubated overnight with primary antibodies against mouse LDLR (Sino Biological, Cat. No. 50305-R032, Clone 032). Secondary antibodies, conjugated with DyLight488 (abcam, Cat. No. ab96883, polyclonal), were added the next day. Confocal microscopy was performed using Leica TCS SP5 laser scanning microscope mounted on a Leica DMI 6000 CS inverted microscope (Leica Microsystems). A 488-nm argon laser was used to excite Alexa 488, and fluorescence emission was measured at 510–550 nm. Leica LAS AF software was used to acquire and process the images.

### Histology of the aortic arch

Preparation of aortic arch cross-sections underwent as previously described.[82–85] After euthanizing the mice, the surface of the mice was rinsed with 70% ethanol. Using forceps and scissors, the skin was cut from the base of the abdomen to the top of the thorax. The ribcage was opened bilaterally until the thymus was exposed. The organs were washed with 10 mL of cold PBS by puncturing the heart apex. Using Moria forceps and Vans scissors, the heart with the aorta was dissected from the diaphragm. Surrounding vessels (left and right carotid artery, left subclavian artery) were cut. The aortic arches were dissected from the heart under a stereomicroscope. The aortic arches were then fixed with 4% formalin solution until further use. The aortic arches were fixed in phosphate-buffered 4% formalin (Sigma Aldrich) for 48 h and then transferred to 70% ethanol until further processing. Before embedding the samples in OCT medium (Leica), they were rinsed three times with PBS for 10 min. They were then transferred to 15% sucrose in 1 × PBS at 4°C until the tissue had sunk. Next, the samples were transferred to 30% sucrose in 1 × PBS at 4°C until the tissue had sunk. Then the samples were snap-frozen in liquid nitrogen and embedded in an OCT compound. The aortic arches were sectioned at 10 μm using a cryostat (Leica). Samples on microscopy slides were stained with Oil Red O (ORO; Sigma Aldrich) and counterstained with Mayer's Hematoxylin solution (Merck). Slides were examined microscopically using the CX7 system (Thermo Fisher) under brightfield illumination (4× objective; camera acquisition mode: 1104*1104 px [2x2 binning]; field size: 2506.08*2508.08 microns). We analyzed 84 images (aortic arches from three mice; two were lost due to technical difficulties) of the pCG1 group and 326 images (aortic arches from five mice) of the chPCSK9-tox group using ImageJ.[75] We performed a color deconvolution algorithm on RGB images to determine hematoxylin staining ([r1] = 0.56925064, [g1] = 0.7286882, [b1] = 0.38074568), ORO staining ([r2] = 0.507444, [g2] = 0.6778302, [b2] = 0.6111796), and background ([r3] = 0.507444, [g3] = 0.55258584, [b3] = 0.661172). Using the thresholding method, the ORO channel was converted into a binary image and was masked to black and white. We measured area of black spots (ORO-staining) in $mm^2$. Aorta sizes (area and diameter) were also measured using ImageJ.[75] Representative slides were stained overnight with Alexa 647-conjugated Mac-3 (CD107b) antibodies (1:200 dilution; BioLegend, cat. no. 108511, clone M3/84). Hoechst 33342 (Immunochemistry Technologies, cat. no. 639) was used as counterstain for nuclei. Confocal microscopy was performed as described above. A 633-nm red laser was used to excite Alexa 647; fluorescence emission detected at 668 nm. A 405-nm violet laser was used to excite Hoechst 33342; fluorescence emission was detected at 461 nm.

### Cytotoxicity of T cells

To determine the absence of PCSK9-specific cytotoxicity, spleens were harvested from immunized mice. Single-cell suspensions were isolated using the tissue dissociator (gentleMACS dissociator) according to the manufacturer's instructions (Miltenyi Biotec). Erythrocytes were lysed with RBC lysis buffer (BioLegend, 420301). After seeding, cells were stimulated with recombinant proteins at a final concentration 10 μg/mL. After 24 h, supernatants were collected for ELISA quantification of cytokines (mIFNγ: Invitrogen 88-7314-88, mIL2: Invitrogen 88-7024-88); 6 to $9*10^6$ spleen cells were used for the flow cytometry analysis. The cells were resuspended in buffer containing 10% of TruStain FcX PLUS (anti-mouse CD16/32; BioLegend 156603). Afterward they were fixed, permeabilized (Cyto-Fast Fix/perm buffer, BioLegend BZ-426803), and stained with antibodies (Table S2). Data were measured on the 3-laser Aurora spectral flow cytometer (Cytek Biosciences) with SpectroFlo v3.1.0 software (Cytek Biosciences). Unstained, single-stained, and FMO samples were used for manual gating in FlowJo software (BD Biosciences).

### Statistical analysis

Analyses were performed using RStudio and GraphPad Prism software. *In vivo* results are expressed as mean ± SEM and other results as mean ± SD. Statistical analyses are indicated in the figure legends; if not stated otherwise, significance was considered for adjusted $p$ value <0.05.

## DATA AVAILABILITY

All authors confirm that all data generated, supporting the findings in this study, is available within the paper and its supplemental figures. RNA-seq data from mouse liver are publicly available and can be viewed in the NCBI Gene Expression Omnibus (GSE282355). All other data are available on request.

## ACKNOWLEDGMENTS

This work was supported by grants from the Slovenian Research and Innovation Agency (P4-0176 [R.J.] and J3-4526 [A.B.]). EU HORIZON-WIDERA CTGCT 101059842 was granted to R.J. We thank K. Podgoršek and A. Perčič for the maintenance of the mouse colony and their technical help with *in vivo* experiments; T. Strmljan and A. Županič for their technical assistance; and T. Železnik Ramuta for help and relevant discussions regarding histological analysis. All schemes were drawn using BioRender.com.

## AUTHOR CONTRIBUTIONS

Š.M., R.J., and D.L. designed the experiments. Š.M., H.E., T.F., and D.L. performed experimental work. D.L., A.G.U., and S.O. performed animal experiments. R.J. and A. B. conceived and supervised the study. All authors analyzed and discussed the results. Š.M. and R.J. wrote the manuscript. All authors discussed and commented on manuscript before submission

## DECLARATION OF INTERESTS

The authors declare no competing interests.

## SUPPLEMENTAL INFORMATION

Supplemental information can be found online at https://doi.org/10.1016/j.omtm.2025.101535.

## REFERENCES


1. Lusis, A.J. (2000). Atherosclerosis. Nature *407*, 233–241. https://doi.org/10.1038/35025203.
2. Nettersheim, F.S., De Vore, L., and Winkels, H. (2020). Vaccination in Atherosclerosis. Cells *9*, 2560. https://doi.org/10.3390/cells9122560.
3. Xu, J., and Shapiro, M.D. (2021). Current Evidence and Future Directions of PCSK9 Inhibition. US Cardiol. *15*, e01. https://doi.org/10.15420/usc.2020.17.
4. Ragusa, R., Basta, G., Neglia, D., De Caterina, R., Del Turco, S., and Caselli, C. (2021). PCSK9 and atherosclerosis: Looking beyond LDL regulation. Eur. J. Clin. Invest. *51*, e13459. https://doi.org/10.1111/eci.13459.
5. Tobert, J.A. (2003). Lovastatin and beyond: the history of the HMG-CoA reductase inhibitors. Nat. Rev. Drug Discov. *2*, 517–526. https://doi.org/10.1038/nrd1112.
6. Kobiyama, K., Saigusa, R., and Ley, K. (2019). Vaccination against Atherosclerosis. Curr. Opin. Immunol. *59*, 15–24. https://doi.org/10.1016/j.coi.2019.02.008.
7. Benjannet, S., Rhainds, D., Essalmani, R., Mayne, J., Wickham, L., Jin, W., Asselin, M.-C., Hamelin, J., Varret, M., Allard, D., et al. (2004). NARC-1/PCSK9 and Its Natural Mutants: Zymogen cleavage and effects on the low density lipoprotein (LDL) receptor and LDL cholesterol. J. Biol. Chem. *279*, 48865–48875. https://doi.org/10.1074/jbc.M409699200.
8. Timms, K.M., Wagner, S., Samuels, M.E., Forbey, K., Goldfine, H., Jammulapati, S., Skolnick, M.H., Hopkins, P.N., Hunt, S.C., and Shattuck, D.M. (2004). A mutation in PCSK9 causing autosomal-dominant hypercholesterolemia in a Utah pedigree. Hum. Genet. *114*, 349–353. https://doi.org/10.1007/s00439-003-1071-9.
9. Benjannet, S., Hamelin, J., Chrétien, M., and Seidah, N.G. (2012). Loss- and Gain-of-function PCSK9 Variants: Cleavage specificity, dominant negative effects, and low density lipoprotein receptor (LDLR) degradation. J. Biol. Chem. *287*, 33745–33755. https://doi.org/10.1074/jbc.M112.399725.
10. Mayne, J., Dewpura, T., Raymond, A., Bernier, L., Cousins, M., Ooi, T.C., Davignon, J., Seidah, N.G., Mbikay, M., and Chrétien, M. (2011). Novel Loss-of-Function PCSK9 Variant Is Associated with Low Plasma LDL Cholesterol in a French-Canadian Family and with Impaired Processing and Secretion in Cell Culture. Clin. Chem. *57*, 1415–1423. https://doi.org/10.1373/clinchem.2011.165191.
11. Zhao, Z., Tuakli-Wosornu, Y., Lagace, T.A., Kinch, L., Grishin, N.V., Horton, J.D., Cohen, J.C., and Hobbs, H.H. (2006). Molecular Characterization of Loss-of-Function Mutations in PCSK9 and Identification of a Compound Heterozygote. Am. J. Hum. Genet. *79*, 514–523. https://doi.org/10.1086/507488.
12. Bao, X., Liang, Y., Chang, H., Cai, T., Feng, B., Gordon, K., Zhu, Y., Shi, H., He, Y., and Xie, L. (2024). Targeting proprotein convertase subtilisin/kexin type 9 (PCSK9): from bench to bedside. Signal Transduct. Target. Ther. *9*, 13–49. https://doi.org/10.1038/s41392-023-01690-3.
13. Katzmann, J.L., Gouni-Berthold, I., and Laufs, U. (2020). PCSK9 Inhibition: Insights From Clinical Trials and Future Prospects. Front. Physiol. *11*, 595819. https://doi.org/10.3389/fphys.2020.595819.
14. Raal, F.J., Kallend, D., Ray, K.K., Turner, T., Koenig, W., Wright, R.S., Wijngaard, P. L.J., Curcio, D., Jaros, M.J., Leiter, L.A., et al. (2020). Inclisiran for the Treatment of Heterozygous Familial Hypercholesterolemia. N. Engl. J. Med. *382*, 1520–1530. https://doi.org/10.1056/NEJMoa1913805.
15. Davis, J.R., Banskota, S., Levy, J.M., Newby, G.A., Wang, X., Anzalone, A.V., Nelson, A.T., Chen, P.J., Hennes, A.D., An, M., et al. (2024). Efficient prime editing in mouse brain, liver and heart with dual AAVs. Nat. Biotechnol. *42*, 253–264. https://doi.org/10.1038/s41587-023-01758-z.
16. Gao, Z., Ravendran, S., Mikkelsen, N.S., Haldrup, J., Cai, H., Ding, X., Paludan, S.R., Thomsen, M.K., Mikkelsen, J.G., and Bak, R.O. (2022). A truncated reverse transcriptase enhances prime editing by split AAV vectors. Mol. Ther. *30*, 2942–2951. https://doi.org/10.1016/j.ymthe.2022.07.001.
17. Link, A., and Bachmann, M.F. (2010). Immunodrugs: breaking B- but not T-cell tolerance with therapeutic anticytokine vaccines. Immunotherapy *2*, 561–574. https://doi.org/10.2217/imt.10.30.
18. Shah, P.K., Chyu, K.-Y., Dimayuga, P.C., and Nilsson, J. (2014). Vaccine for Atherosclerosis. J. Am. Coll. Cardiol. *64*, 2779–2791. https://doi.org/10.1016/j.jacc.2014.10.018.
19. Barabas, A.Z., Barabas, A.D., Cole, C.D., Weir, D.M., and Lafreniere, R. (2011). Four Aspects of Autoimmunity and How to Regain Tolerance to Self From an Autoimmune Disease Utilizing the Modified Vaccination Technique. In Autoimmune Disorders - Current Concepts and Advances from Bedside to Mechanistic Insights, F.-P. Huang, ed. (InTech). https://doi.org/10.5772/20668.
20. Ahmad, T.A., Eweida, A.E., and El-Sayed, L.H. (2016). T-cell epitope mapping for the design of powerful vaccines. Vaccine Rep. *6*, 13–22. https://doi.org/10.1016/j.vacrep.2016.07.002.
21. Kanduc, D. (2009). Epitopic peptides with low similarity to the host proteome: towards biological therapies without side effects. Expert Opin. Biol. Ther. *9*, 45–53. https://doi.org/10.1517/14712590802614041.
22. Galabova, G., Brunner, S., Winsauer, G., Juno, C., Wanko, B., Mairhofer, A., Lührs, P., Schneeberger, A., von Bonin, A., Mattner, F., et al. (2014). Peptide-Based Anti-PCSK9 Vaccines - An Approach for Long-Term LDLc Management. PLoS One *9*, e114469.
23. Crossey, E., Amar, M.J.A., Sampson, M., Peabody, J., Schiller, J.T., Chackerian, B., and Remaley, A.T. (2015). A cholesterol-lowering VLP vaccine that targets PCSK9. Vaccine *33*, 5747–5755. https://doi.org/10.1016/j.vaccine.2015.09.044.
24. Pan, Y., Zhou, Y., Wu, H., Chen, X., Hu, X., Zhang, H., Zhou, Z., Qiu, Z., and Liao, Y. (2017). A Therapeutic Peptide Vaccine Against PCSK9. Sci. Rep. *7*, 12534. https://doi.org/10.1038/s41598-017-13069-w.
25. Vroom, M.M., Lu, H., Lewis, M., Thibodeaux, B.A., Brooks, J.K., Longo, M.S., Ramos, M.M., Sahni, J., Wiggins, J., Boyd, J.D., et al. (2024). VXX-401, a novel anti-PCSK9 vaccine, reduces LDL-C in cynomolgus monkeys. J. Lipid Res. *65*, 100497. https://doi.org/10.1016/j.jlr.2024.100497.
26. Fowler, A., Van Rompay, K.K.A., Sampson, M., Leo, J., Watanabe, J.K., Usachenko, J.L., Immareddy, R., Lovato, D.M., Schiller, J.T., Remaley, A.T., and Chackerian, B. (2023). A virus-like particle-based bivalent PCSK9 vaccine lowers LDL-cholesterol levels in non-human primates. NPJ Vaccines *8*, 142. https://doi.org/10.1038/s41541-023-00743-6.
27. Ols, S., Lenart, K., Arcoverde Cerveira, R., Miranda, M.C., Brunette, N., Kochmann, J., Corcoran, M., Skotheim, R., Philomin, A., Cagigi, A., et al. (2023). Multivalent antigen display on nanoparticle immunogens increases B cell clonotype diversity and neutralization breadth to pneumoviruses. Immunity *56*, 2425–2441.e14. https://doi.org/10.1016/j.immuni.2023.08.011.
28. Vita, R., Mahajan, S., Overton, J.A., Dhanda, S.K., Martini, S., Cantrell, J.R., Wheeler, D.K., Sette, A., and Peters, B. (2019). The Immune Epitope Database (IEDB): 2018 update. Nucleic Acids Res. *47*, D339–D343. https://doi.org/10.1093/nar/gky1006.
29. Karosiene, E., Lundegaard, C., Lund, O., and Nielsen, M. (2012). NetMHCcons: a consensus method for the major histocompatibility complex class I predictions. Immunogenetics *64*, 177–186. https://doi.org/10.1007/s00251-011-0579-8.
30. Andreatta, M., and Nielsen, M. (2016). Gapped sequence alignment using artificial neural networks: application to the MHC class I system. Bioinformatics *32*, 511–517. https://doi.org/10.1093/bioinformatics/btv639.
31. Larsen, M.V., Lundegaard, C., Lamberth, K., Buus, S., Lund, O., Nielsen, M., DTU, H.T., Larsen, M.V., Lundegaard, C., Lamberth, K., et al. (2007). Large-scale validation of methods for cytotoxic T-lymphocyte epitope prediction. BMC Bioinf. *8*, 424. https://doi.org/10.1186/1471-2105-8-424.
32. DeVette, C.I., Andreatta, M., Bardet, W., Cate, S.J., Jurtz, V.I., Jackson, K.W., Welm, A.L., Nielsen, M., and Hildebrand, W.H. (2018). NetH2pan: A Computational Tool to Guide MHC Peptide Prediction on Murine Tumors. Cancer Immunol. Res. *6*, 636–644. https://doi.org/10.1158/2326-6066.CIR-17-0298.
33. Jumper, J., Evans, R., Pritzel, A., Green, T., Figurnov, M., Ronneberger, O., Tunyasuvunakool, K., Bates, R., Žídek, A., Potapenko, A., et al. (2021). Highly accurate protein structure prediction with AlphaFold. Nature *596*, 583–589. https://doi.org/10.1038/s41586-021-03819-2.

34. Abramson, J., Adler, J., Dunger, J., Evans, R., Green, T., Pritzel, A., Ronneberger, O., Willmore, L., Ballard, A.J., Bambrick, J., et al. (2024). Accurate structure prediction of biomolecular interactions with AlphaFold 3. Nature *630*, 493–500. https://doi.org/10.1038/s41586-024-07487-w.

35. Slingluff, C.L., Jr., Yamshchikov, G., Neese, P., Galavotti, H., Eastham, S., Engelhard, V.H., Kittlesen, D., Deacon, D., Hibbitts, S., Grosh, W.W., et al. (2001). Phase I trial of a melanoma vaccine with gp100(280-288) peptide and tetanus helper peptide in adjuvant: immunologic and clinical outcomes. Clin. Cancer Res. *7*, 3012–3024.

36. Diethelm-Okita, B.M., Okita, D.K., Banaszak, L., and Conti-Fine, B.M. (2000). Universal Epitopes for Human CD4+ Cells on Tetanus and Diphtheria Toxins. J. Infect. Dis. *181*, 1001–1009. https://doi.org/10.1086/315324.

37. Lainščcek, D., Fink, T., Forstnerič, V., Hafner-Bratkovič, I., Orehek, S., Strmšek, Ž., Manček-Keber, M., Pečan, P., Esih, H., Malenšek, Š., et al. (2021). A Nanoscaffolded Spike-RBD Vaccine Provides Protection against SARS-CoV-2 with Minimal Anti-Scaffold Response. Vaccines *9*, 431. https://doi.org/10.3390/vaccines9050431.

38. Fattori, E., Cappelletti, M., Lo Surdo, P., Calzetta, A., Bendtsen, C., Ni, Y.G., Pandit, S., Sitlani, A., Mesiti, G., Carfí, A., and Monaci, P. (2012). Immunization against proprotein convertase subtilisin-like/kexin type 9 lowers plasma LDL-cholesterol levels in mice. J. Lipid Res. *53*, 1654–1661. https://doi.org/10.1194/jlr.M028340.

39. Lo Sasso, G., Schlage, W.K., Boué, S., Veljkovic, E., Peitsch, M.C., and Hoeng, J. (2016). The Apoe−/− mouse model: a suitable model to study cardiovascular and respiratory diseases in the context of cigarette smoke exposure and harm reduction. J. Transl. Med. *14*, 146. https://doi.org/10.1186/s12967-016-0901-1.

40. Zhang, S.H., Reddick, R.L., Piedrahita, J.A., and Maeda, N. (1992). Spontaneous Hypercholesterolemia and Arterial Lesions in Mice Lacking Apolipoprotein E. Science *258*, 468–471. https://doi.org/10.1126/science.1411543.

41. Oppi, S., Lüscher, T.F., and Stein, S. (2019). Mouse Models for Atherosclerosis Research—Which Is My Line? Front. Cardiovasc. Med. *6*, 46. https://doi.org/10.3389/fcvm.2019.00046.

42. Véniant, M.M., Withycombe, S., and Young, S.G. (2001). Lipoprotein Size and Atherosclerosis Susceptibility in Apoe−/− and Ldlr−/− Mice. Arterioscler. Thromb. Vasc. Biol. *21*, 1567–1570. https://doi.org/10.1161/hq1001.097780.

43. Nakashima, Y., Plump, A.S., Raines, E.W., Breslow, J.L., and Ross, R. (1994). ApoE-deficient mice develop lesions of all phases of atherosclerosis throughout the arterial tree. Arteriosclerosis and Thrombosis. Arterioscler. Thromb. *14*, 133–140. https://doi.org/10.1161/01.ATV.14.1.133.

44. Liu, B., Fang, L., Mo, P., Chen, C., Ji, Y., Pang, L., Chen, H., Deng, Y., Ou, W., and Liu, S.-M. (2023). Apoe-knockout induces strong vascular oxidative stress and significant changes in the gene expression profile related to the pathways implicated in redox, inflammation, and endothelial function. Cell. Signal. *108*, 110696. https://doi.org/10.1016/j.cellsig.2023.110696.

45. Frey, A., Di Canzio, J., and Zurakowski, D. (1998). A statistically defined endpoint titer determination method for immunoassays. J. Immunol. Methods *221*, 35–41. https://doi.org/10.1016/s0022-1759(98)00170-7.

46. Matyas, C., Trojnar, E., Zhao, S., Arif, M., Mukhopadhyay, P., Kovacs, A., Fabian, A., Tokodi, M., Bagyura, Z., Merkely, B., et al. (2023). PCSK9, A Promising Novel Target for Age-Related Cardiovascular Dysfunction. JACC. Basic Transl. Sci. *8*, 1334–1353. https://doi.org/10.1016/j.jacbts.2023.06.005.

47. Liu, C., Schönke, M., Zhou, E., Li, Z., Kooijman, S., Boon, M.R., Larsson, M., Wallenius, K., Dekker, N., Barlind, L., et al. (2021). Pharmacological treatment with FGF21 strongly improves plasma cholesterol metabolism to reduce atherosclerosis. Cardiovasc. Res. *118*, 489–502. https://doi.org/10.1093/cvr/cvab076.

48. Kokkinos, J., Tang, S., Rye, K.-A., and Ong, K.L. (2017). The role of fibroblast growth factor 21 in atherosclerosis. Atherosclerosis *257*, 259–265. https://doi.org/10.1016/j.atherosclerosis.2016.11.033.

49. Lin, Z., Pan, X., Wu, F., Ye, D., Zhang, Y., Wang, Y., Jin, L., Lian, Q., Huang, Y., Ding, H., et al. (2015). Fibroblast Growth Factor 21 Prevents Atherosclerosis by Suppression of Hepatic Sterol Regulatory Element-Binding Protein-2 and Induction of Adiponectin in Mice. Circulation *131*, 1861–1871. https://doi.org/10.1161/CIRCULATIONAHA.115.015308.

50. Kuchibhotla, S., Vanegas, D., Kennedy, D.J., Guy, E., Nimako, G., Morton, R.E., and Febbraio, M. (2008). Absence of CD36 protects against atherosclerosis in ApoE knock-out mice with no additional protection provided by absence of scavenger receptor A I/II. Cardiovasc. Res. *78*, 185–196. https://doi.org/10.1093/cvr/cvm093.

51. Feng, Y., Sun, W., Sun, F., Yin, G., Liang, P., Chen, S., Liu, X., Jiang, T., and Zhang, F. (2022). Biological Mechanisms and Related Natural Inhibitors of CD36 in Nonalcoholic Fatty Liver. Drug Des. Devel. Ther. *16*, 3829–3845. https://doi.org/10.2147/DDDT.S386982.

52. Demers, A., Samami, S., Lauzier, B., Des Rosiers, C., Ngo Sock, E.T., Ong, H., and Mayer, G. (2015). PCSK9 Induces CD36 Degradation and Affects Long-Chain Fatty Acid Uptake and Triglyceride Metabolism in Adipocytes and in Mouse Liver. Arterioscler. Thromb. Vasc. Biol. *35*, 2517–2525. https://doi.org/10.1161/ATVBAHA.115.306032.

53. Sesterhenn, F., Yang, C., Bonet, J., Cramer, J.T., Wen, X., Wang, Y., Chiang, C.-I., Abriata, L.A., Kucharska, I., Castoro, G., et al. (2020). De novo protein design enables the precise induction of RSV-neutralizing antibodies. Science *368*, eaay5051. https://doi.org/10.1126/science.aay5051.

54. Goksøyr, L., Skrzypczak, M., Sampson, M., Nielsen, M.A., Salanti, A., Theander, T. G., Remaley, A.T., De Jongh, W.A., and Sander, A.F. (2022). A cVLP-Based Vaccine Displaying Full-Length PCSK9 Elicits a Higher Reduction in Plasma PCSK9 Than Similar Peptide-Based cVLP Vaccines. Vaccines (Basel) *11*, 2. https://doi.org/10.3390/vaccines11010002.

55. Wang, C., and Yuan, F. (2024). A comprehensive comparison of DNA and RNA vaccines. Adv. Drug Deliv. Rev. *210*, 115340. https://doi.org/10.1016/j.addr.2024.115340.

56. Sumida, K.H., Núñez-Franco, R., Kalvet, I., Pellock, S.J., Wicky, B.I.M., Milles, L.F., Dauparas, J., Wang, J., Kipnis, Y., Jameson, N., et al. (2024). Improving Protein Expression, Stability, and Function with ProteinMPNN. J. Am. Chem. Soc. *146*, 2054–2061. https://doi.org/10.1021/jacs.3c10941.

57. Watson, J.L., Juergens, D., Bennett, N.R., Trippe, B.L., Yim, J., Eisenach, H.E., Ahern, W., Borst, A.J., Ragotte, R.J., Milles, L.F., et al. (2023). De novo design of protein structure and function with RFdiffusion. Nature *620*, 1089–1100. https://doi.org/10.1038/s41586-023-06415-8.

58. Wu, K.E., Yang, K.K., Berg, R. van den, Zou, J., Lu, A.X., and Amini, A.P. (2022). Protein structure generation via folding diffusion. Nat. Commun. *15*, 1059.

59. King, C., Garza, E.N., Mazor, R., Linehan, J.L., Pastan, I., Pepper, M., and Baker, D. (2014). Removing T-cell epitopes with computational protein design. Proc. Natl. Acad. Sci. USA *111*, 8577–8582. https://doi.org/10.1073/pnas.1321126111.

60. Mashraqi, M.M., Alzamami, A., Alturki, N.A., Almasaudi, H.H., Ahmed, I., Alshamrani, S., and Basharat, Z. (2023). Chimeric vaccine design against the conserved TonB-dependent receptor-like β-barrel domain from the outer membrane tbpA and hpuB proteins of Kingella kingae ATCC 23330. Front. Mol. Biosci. *10*, 1258834. https://doi.org/10.3389/fmolb.2023.1258834.

61. Gasser, H.-C., Oyarzún, D.A., Alfaro, J., and Rajan, A. (2024). Integrating MHC Class I visibility targets into the ProteinMPNN protein design process. Preprint at bioRxiv. https://doi.org/10.1101/2024.06.04.597365.

62. Lee, Y.T., Lin, H.Y., Chan, Y.W.F., Li, K.H.C., To, O.T.L., Yan, B.P., Liu, T., Li, G., Wong, W.T., Keung, W., and Tse, G. (2017). Mouse models of atherosclerosis: a historical perspective and recent advances. Lipids Health Dis. *16*, 12. https://doi.org/10.1186/s12944-016-0402-5.

63. Getz, G.S., and Reardon, C.A. (2012). Animal models of atherosclerosis. Arterioscler. Thromb. Vasc. Biol. *32*, 1104–1115. https://doi.org/10.1161/ATVBAHA.111.237693.

64. Musunuru, K., Chadwick, A.C., Mizoguchi, T., Garcia, S.P., DeNizio, J.E., Reiss, C. W., Wang, K., Iyer, S., Dutta, C., Clendaniel, V., et al. (2021). In vivo CRISPR base editing of PCSK9 durably lowers cholesterol in primates. Nature *593*, 429–434. https://doi.org/10.1038/s41586-021-03534-y.

65. Tremblay, F., Xiong, Q., Shah, S.S., Ko, C.-W., Kelly, K., Morrison, M.S., Giancarlo, C., Ramirez, R.N., Hildebrand, E.M., Voytek, S.B., et al. (2025). A potent epigenetic editor targeting human PCSK9 for durable reduction of low-density lipoprotein cholesterol levels. Nat. Med. *31*, 1329–1338. https://doi.org/10.1038/s41591-025-03508-x.

66. UniProt Consortium (2023). UniProt: the Universal Protein Knowledgebase in 2023. Nucleic Acids Res. *51*, D523–D531. https://doi.org/10.1093/nar/gkac1052.

67. Sievers, F., Wilm, A., Dineen, D., Gibson, T.J., Karplus, K., Li, W., Lopez, R., McWilliam, H., Remmert, M., Söding, J., et al. (2011). Fast, scalable generation of high-quality protein multiple sequence alignments using Clustal Omega. Mol. Syst. Biol. *7*, 539. https://doi.org/10.1038/msb.2011.75.

68. Pettersen, E.F., Goddard, T.D., Huang, C.C., Couch, G.S., Greenblatt, D.M., Meng, E.C., and Ferrin, T.E. (2004). UCSF Chimera–a visualization system for exploratory research and analysis. J. Comput. Chem. *25*, 1605–1612. https://doi.org/10.1002/jcc.20084.

69. Sanner, M.F., Olson, A.J., and Spehner, J.C. (1996). Reduced surface: an efficient way to compute molecular surfaces. Biopolymers *38*, 305–320. https://doi.org/10.1002/(SICI)1097-0282(199603)38:3%3C305::AID-BIP4%3E3.0.CO;2-Y.

70. Mirdita, M., Ovchinnikov, S., and Steinegger, M. (2021). ColabFold - Making Protein folding accessible to all. Preprint at bioRxiv. https://doi.org/10.1101/2021.08.15.456425.

71. Bjørklund, M.M., Hollensen, A.K., Hagensen, M.K., Dagnaes-Hansen, F., Christoffersen, C., Mikkelsen, J.G., and Bentzon, J.F. (2014). Induction of atherosclerosis in mice and hamsters without germline genetic engineering. Circ. Res. *114*, 1684–1689. https://doi.org/10.1161/CIRCRESAHA.114.302937.

72. Li, J.J., Liu, J., Lupino, K., Liu, X., Zhang, L., and Pei, L. (2018). Growth Differentiation Factor 15 Maturation Requires Proteolytic Cleavage by PCSK3, -5, and -6. Mol. Cell. Biol. *38*, e00249-18. https://doi.org/10.1128/MCB.00249-18.

73. Jenkins, B., Decker, H., Bentley, M., Luisi, J., and Banker, G. (2012). A novel split kinesin assay identifies motor proteins that interact with distinct vesicle populations. J. Cell Biol. *198*, 749–761. https://doi.org/10.1083/jcb.201205070.

74. Hoffmann, M., Kleine-Weber, H., Schroeder, S., Krüger, N., Herrler, T., Erichsen, S., Schiergens, T.S., Herrler, G., Wu, N.-H., Nitsche, A., et al. (2020). SARS-CoV-2 Cell Entry Depends on ACE2 and TMPRSS2 and Is Blocked by a Clinically Proven Protease Inhibitor. Cell *181*, 271–280.e8. https://doi.org/10.1016/j.cell.2020.02.052.

75. Schindelin, J., Arganda-Carreras, I., Frise, E., Kaynig, V., Longair, M., Pietzsch, T., Preibisch, S., Rueden, C., Saalfeld, S., Schmid, B., et al. (2012). Fiji: an open-source platform for biological-image analysis. Nat. Methods *9*, 676–682. https://doi.org/10.1038/nmeth.2019.

76. Martin, M. (2011). Cutadapt removes adapter sequences from high-throughput sequencing reads. EMBnet. J. *17*, 10–12. https://doi.org/10.14806/ej.17.1.200.

77. Teichman, G., Cohen, D., Ganon, O., Dunsky, N., Shani, S., Gingold, H., and Rechavi, O. (2023). RNAlysis: analyze your RNA sequencing data without writing a single line of code. BMC Biol. *21*, 74. https://doi.org/10.1186/s12915-023-01574-6.

78. Bray, N.L., Pimentel, H., Melsted, P., and Pachter, L. (2016). Near-optimal probabilistic RNA-seq quantification. Nat. Biotechnol. *34*, 525–527. https://doi.org/10.1038/nbt.3519.

79. Love, M.I., Huber, W., and Anders, S. (2014). Moderated estimation of fold change and dispersion for RNA-seq data with DESeq2. Genome Biol. *15*, 550. https://doi.org/10.1186/s13059-014-0550-8.

80. Blighe, K., Rana, S., and Lewis, M. (2025). EnhancedVolcano: publication-ready volcano plots with enhanced colouring and labeling. https://doi.org/10.18129/B9.bioc.EnhancedVolcano.

81. Liao, Y., Wang, J., Jaehnig, E.J., Shi, Z., and Zhang, B. (2019). WebGestalt 2019: gene set analysis toolkit with revamped UIs and APIs. Nucleic Acids Res. *47*, W199–W205. https://doi.org/10.1093/nar/gkz401.

82. Andrés-Manzano, M.J., Andrés, V., and Dorado, B. (2015). Oil Red O and Hematoxylin and Eosin Staining for Quantification of Atherosclerosis Burden in Mouse Aorta and Aortic Root. Methods Mol. Biol. *1339*, 85–99. https://doi.org/10.1007/978-1-4939-2929-0_5.

83. Venegas-Pino, D.E., Banko, N., Khan, M.I., Shi, Y., and Werstuck, G.H. (2013). Quantitative Analysis and Characterization of Atherosclerotic Lesions in the Murine Aortic Sinus. JoVE J. *82*, e50933. https://doi.org/10.3791/50933.

84. Baglione, J., and Smith, J.D. (2007). Quantitative Assay for Mouse Atherosclerosis in the Aortic Root. In Cardiovascular Disease: Methods and Protocols Volume 2: Molecular Medicine Methods in Molecular Medicine, Q.K. Wang, ed. (Humana Press), pp. 83–95. https://doi.org/10.1385/1-59745-213-0:83.

85. Štrbenc, M., Klenovšek, K.K., and Majdič *, G. (2023). Female gonadal hormones are a risk for developing atherosclerotic changes in C57BL/6J mice on atherogenic diet. Slovenian Vet. Res. *60*, 55–66. https://doi.org/10.26873/SVR-1519-2023.